J. Fluid Mech. (2007), *vol.* 577, *pp.* 79–104.
doi:10.1017/S0022112006004320 Printed in the United Kingdom

Three-dimensional transition in the wake of a transversely oscillating cylinder

JUSTIN S. LEONTINI, M. C. THOMPSON AND K. HOURIGAN

Fluids Laboratory for Aeronautical and Industrial Research (FLAIR), Department of Mechanical Engineering, Monash University, Melbourne, Victoria 3800, Australia

(Received 29 May 2006 and in revised form 18 October 2006)

A Floquet stability analysis of the transition to three-dimensionality in the wake of a cylinder forced to oscillate transversely to the free stream has been undertaken. The effect of varying the oscillation amplitude is determined for a frequency of oscillation close to the natural shedding frequency. The three-dimensional modes that arise are identified, and the effect of the oscillation amplitude on their structure and growth rate quantified.

It is shown that when the two-dimensional wake is in the $2S$ configuration (which is similar to the Kármán vortex street), the three-dimensional modes that arise are similar in nature and symmetry structure to the modes in the wake of a fixed cylinder. These modes are known as modes A, B and QP and occur in this order with increasing Re. However, increasing the amplitude of oscillation causes the critical Reynolds number for mode A to increase significantly, to the point where mode B becomes critical before mode A. The critical wavelength for mode A is also affected by the oscillation, becoming smaller with increasing amplitude. Elliptic instability theory is shown also to predict this trend, providing further support that mode A primarily arises as a result of an elliptic instability.

At higher oscillation amplitudes, the spatio-temporal symmetry of the two-dimensional wake changes and it takes on the $P + S$ configuration, with a pair of vortices on one side of the wake and a single vortex on the other side, for each oscillation cycle. With the onset of this configuration, modes A, B and QP cease to exist. It is shown that two new three-dimensional modes arise from this base flow, which we call modes SL and SS. Both of these modes are subharmonic, repeating over two base-flow periods. Also, either mode can be the first to become critical, depending on the amplitude of oscillation of the cylinder.

The emergence of these two new modes, as well as the reversal of the order of inception of the three-dimensional modes A and B, leads to the observation that for an oscillating cylinder wake there are four different modes that can lead the transition to three-dimensionality, depending on the amplitude of oscillation. Therefore this type of flow provides a good example for studying the effect of mode-order inception on the path taken to turbulence in bluff-body wakes.

For the range of amplitudes studied, the maximum Re value for which the flow remains two-dimensional is 280.

1. Introduction

It is known that the onset of three-dimensionality in a cylinder wake can be delayed if the cylinder is forced to oscillate transversely to the free stream at moderate

amplitudes. Experiments with an elongated cylinder by Berger (1967) showed that suitable transverse oscillations extended the upper limit of the laminar shedding regime, from the non-oscillating limit until Reynolds number $300 \sim 350$. Koopman (1967) and Griffin (1971) both performed forced-oscillation experiments at $Re \leqslant 300$ on the assumption that a laminar shedding regime persist over this Re range. The visualizations of vortex filaments shed from an transversely oscillating cylinder by Koopman (1967) at $Re = 200$ showed no spanwise variation. This two-dimensionality is assumed to be attributable to the oscillation, as the more recent work of Williamson (1996*b*) and Barkley & Henderson (1996) has shown that the transition to three-dimensional flow occurs prior to $Re = 200$ for a stationary cylinder.

While the phenomenon of the delay of three-dimensionality for oscillating cylinders is well known, it has not previously been quantified. The primary aim of this paper is to evaluate the effect of transverse oscillations on the onset of three-dimensionality in a circular cylinder wake.

The obvious reference case for such a study is provided by the limiting case of a stationary cylinder. For the latter the transition from the two-dimensional Kármán vortex street to three-dimensional flow occurs with the onset of the first three-dimensional mode, aptly named mode A, at $Re \simeq 190$, first described in detail by Williamson (1988). It has been shown that this mode in a pure form breaks only the translational and span-invariant reflectional symmetry of the two-dimensional flow; it preserves the spatio-temporal symmetry of the two-dimensional base flow (Barkley & Henderson 1996; Barkley, Tuckerman & Golubitsky 2000; Blackburn, Marques & Lopez 2005).

Two other three-dimensional modes have been shown to be theoretically possible: mode B, a second three-dimensional mode, which has a much shorter spanwise wavelength than mode A and breaks the spatio-temporal symmetry as well as the spanwise symmetry of the flow, and mode QP, which is quasi-periodic (hence the designation QP) and consists of modulated travelling or standing waves.

Mode B is predicted to bifurcate from the two-dimensional base flow at $Re \simeq 260$, but experimentally it is observed at lower Re owing to the modification of the two-dimensional base flow by mode A. As Re increases, the saturated mode-B state is seen to dominate the three-dimensional flow, with evidence of mode-B vortical structures still present at $Re > 1000$ (Wu *et al.* 1996). Mode QP has only recently been identified and classified as quasi-periodic by Blackburn & Lopez (2003). Floquet stability analysis shows that this mode becomes unstable at $Re \simeq 377$. However, in reality the wake at this Re is already highly three-dimensional and has descended into spatio-temporal chaos (Henderson 1997), and mode B continues to dominate.

While the possible modes that can occur are now relatively well defined, the physical nature of the instabilities that cause them is less well understood. Williamson (1996*a*) proposed that mode A was due to an elliptic instability of the primary vortex cores and that mode B was due to an instability of the braid shear layers. Subsequently, Leweke & Williamson (1998) showed that elliptic instability theory predicted the wavelength of mode A to within 25 %, and hypothesized that mode B was caused by a hyperbolic instability of the braid shear layers. Later, the Floquet analysis and three-dimensional direct simulations of Thompson, Leweke & Williamson (2001) showed strong evidence that the transition to mode A could be interpreted as a cooperative elliptic instability. The results of the current study add support to this theory.

Floquet stability analysis is well suited to establishing the Re value at which a two-dimensional flow will first become three-dimensional. Barkley & Henderson (1996) first used this method to predict the critical Re value and the wavelengths of

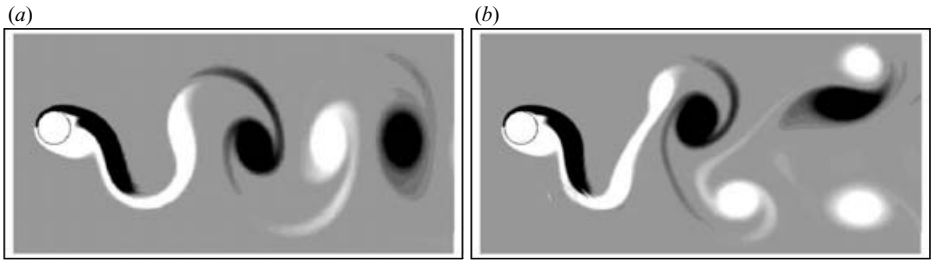

FIGURE 1. (*a*) The Kármán or 2*S* wake, with two single vortices shed per oscillation period: $A^* = 0.6$, $Re = 240$. (*b*) The $P + S$ wake, with one pair of vortices plus one single vortex per oscillation period: $A^* = 0.6$, $Re = 260$. The loss in symmetry compared with the 2*S* wake is evident.

both modes A and B for a fixed cylinder wake. Other bluff-body wakes have been investigated using this method, including square cylinders (Robichaux, Balachandar & Vanka 1999), normal flat plates (Julien, Ortiz & Chomaz 2004), elliptical leading-edge plates (Ryan, Thompson & Hourigan 2005) and tori (Sheard, Thompson & Hourigan 2003). The same method is applied in the current study.

A primary difference between many other flows and that studied in this paper is that most fixed bluff-body flows have only one independent parameter, *Re*, whereas the oscillating cylinder flow considered here has up to three. They are $Re = UD/\nu$, $A^* = A/D$ and the non-dimensional oscillation frequency $f^* = f/UD$, where U is the freestream velocity, D is the cylinder diameter, ν is the kinematic viscosity, A is the amplitude of oscillation (resulting in a peak-to-peak transverse movement $2A$ of the centre of the cylinder) and f is the frequency of oscillation. For the present study, f^* was fixed and only the effect of varying *Re* and A^* was considered. The study of the flow past tori shares this feature of multiple control parameters, the second independent parameter being the diameter ratio (the ratio of the ring diameter and the cylinder cross-section diameter), as does the flow past elliptical leading-edge plates, since the aspect ratio can be varied.

The introduction of a second variable greatly increases the complexity of the bifurcation problem as well as allowing other types of generic bifurcation (Blackburn *et al.* 2005; Marques, Lopez & Blackburn 2004). While the occurrence of different three-dimensional modes is highly unlikely if the two-dimensional wake configuration stays the same, different modes may be possible if the two-dimensional wake symmetries change. Indeed, a change in the two-dimensional wake occurs in the wake of an oscillating cylinder with the onset of the $P + S$ wake configuration; this breaks the spatio-temporal symmetry of the conventional Kármán wake (Williamson & Roshko 1988). Blackburn & Henderson (1999) in a numerical simulation found wakes in this configuration for the oscillating cylinder, even for values of A^* as low as 0.25. With the onset of this different two-dimensional wake, different three-dimensional modes, such as subharmonics, become possible. Shown in figure 1 are examples of the 2*S* wake (the notation indicates the two singular vortices that are shed per oscillation period) and the $P+S$ wake (the notation indicates a configuration where a pair of vortices and one single vortex are shed per oscillation period).

In any bifurcation and stability analysis, symmetry and the symmetries broken by bifurcation play a critical role (Iooss & Joseph 1990). Therefore, it is important to know the symmetry group of the base flow when making this analysis. The two-dimensional vortex street behind a fixed cylinder possesses a translational and

reflectional symmetry along the span, hence it possesses $O(2)$ symmetry. It also possesses a spatio-temporal symmetry, which consists of a reflection about the wake centreline plus a temporal evolution of half a period. This also gives it Z_2 symmetry. Therefore, the total symmetry group of the fixed cylinder wake is expressed as $Z_2 \times O(2)$.

At low amplitudes of oscillation, the oscillating-cylinder wake has the same symmetry group for the base flow. Considering this, along with the fact that the extra variable of cylinder oscillation allows different bifurcations, the following questions arise.

- Which three-dimensional modes occur?
- In what order, with respect to Re and A^*, do these modes occur?
- How does the loss of spatio-temporal symmetry (of the base flow) at higher amplitudes of oscillation affect the transition to three-dimensionality?

Resolved two-dimensional direct simulations and Floquet stability analysis are used to answer these questions.

The structure of the paper is as follows. Sections 2–4 provide a brief overview of the stability theory, numerical methods and validation and a concise description of the problem being studied. The results are presented in § 5, beginning with an Re–A^* parameter map that provides an overview of the key regions and transitions. Following this, the five instability modes are examined separately in more detail. We then provide a broad overview of the main findings and results and conclude with a recap of the most important points.

2. Numerical formulation

2.1. *The spectral-element method*

The simulations utilized a non-deformable mesh fixed to the cylinder, with an extra non-inertial acceleration term added to the Navier–Stokes equations to account for the acceleration of the cylinder across the flow. This approach is more efficient than employing a deforming mesh to account for movement of the cylinder. The extra term is simply added to the right-hand side of the Navier–Stokes equations as a time derivative of the cylinder velocity. This renders the system to be solved as

$$\frac{\partial \boldsymbol{u}}{\partial \tau} = -(\boldsymbol{u}\cdot\nabla)\boldsymbol{u} + \nabla P + \frac{1}{Re}(\nabla^2 \boldsymbol{u}) - \frac{\partial \boldsymbol{u}_{cyl}}{\partial \tau} \tag{2.1}$$

where $\boldsymbol{u}$ is the velocity vector field, τ is the non-dimensional time variable, P is the scalar pressure field and $\boldsymbol{u}_{cyl}$ is the cylinder velocity vector.

The simulations were performed using a spectral-element method for the spatial discretization. This method is described in detail in Karniadakis & Sherwin (2005), and the implementation used here follows that of Thompson *et al.* (1996). The spectral-element method is based on the Galerkin finite-element method, employing high-order Lagrangian-polynomial shape functions within each element. The node points of these Lagrangian polynomials coincide with the Gauss–Lobatto–Legendre quadrature points. This leads to efficient and accurate integrations over each element. This same spatial discretization was used for the base flow and for the evolution of the perturbation fields.

Time advancement was dealt with using a high-order three-step time-splitting scheme. The three steps account for the advection and cylinder-movement pressure terms, the term and the diffusion term of the Navier–Stokes equations. This allows different integration methods to be employed for the linear and nonlinear terms. The nonlinear advection term, including the additional term for the cylinder acceleration

in (2.1), was treated explicitly using a third-order Adams–Bashforth method. The pressure field was evaluated by taking the divergence of the equation for pressure, thus forming a poission equation, and enforcing continuity at the end of the substep. Finally, the diffusion term was evaluated using a Crank–Nicholson scheme applied to the Helmholtz equation. Further details of this time-splitting scheme can be found in Thompson *et al.* (1996), Karniadakis, Israeli & Orszag (1991), and Karniadakis & Henderson (1998).

The boundary conditions in the non-inertial frame were such that the velocity was zero at the cylinder wall and, at the external boundaries of the domain, the crossflow component was equal to the negative of the cylinder velocity. To obtain the pressure boundary conditions, it was assumed that the normal component of the velocity at the end of the pressure substep was equal to the normal component of the freestream velocity, which included the contribution from the cylinder oscillation. This resulted in a first-order Neumann boundary condition for the pressure (Karniadakis *et al.* 1991).

2.2. *Floquet stability analysis*

Linear Floquet stability analysis is a method for determining the stability of periodic solutions. It has been successfully employed for the wakes of bluff bodies, including cylinders (Barkley & Henderson 1996; Blackburn *et al.* 2005), perpendicular plates (Julien *et al.* 2004), tori (Sheard *et al.* 2003) and elliptical leading-edge plates (Ryan *et al.* 2005). The implementation used for the current study has been shown to be effective by Thompson, Leweke & Williamson (2001), Sheard *et al.* (2003) and Ryan *et al.* (2005). Explanations of the basic method can be found in Iooss & Joseph (1990) and Seydel (1994).

In effect, the approach is as follows. Equations that describe the perturbation field are formed by substituting $\boldsymbol{U}(x, y, t) + \boldsymbol{u}'(x, y, z, t)$ for $\boldsymbol{u}(x, y, z, t)$ in the Navier–Stokes equations, where $\boldsymbol{u}$ is the two-dimensional base-flow velocity vector and $\boldsymbol{u}'$ is the three-dimensional perturbation velocity vector. A similar expansion is followed for the pressure. The original equations describing the two-dimensional base flow are then subtracted, and what is left are equations describing the evolution of the perturbation field. The equations are then linearized, since perturbations must grow from low amplitudes where nonlinear terms are negligible. Even though the resulting linear equations describe the perturbation-field evolution only, these equations still rely on the base-flow fields.

The linear perturbation equations can be solved in all three spatial dimensions directly; however, the partial differential equations are linear and have constant coefficients with respect to z, and hence the z (spanwise) dependence for each perturbation field can be expressed as a sum of Fourier modes. Moreover, the solution corresponding to each Fourier mode can be calculated independently.

Floquet theory then looks for solutions of the (two-dimensional) perturbation fields for each spanwise wavelength λ in the form

$$r'(t + T, x, y) = \exp(\sigma T)\, r'(t, x, y). \tag{2.2}$$

Here, r' represents any of the perturbation fields (Floquet modes), t is time and T is the period of the base flow. A Floquet mode is effectively a solution of the perturbation equations with the prescribed spatial wavelength. As the above equation is effectively an eigenvalue problem, there are infinitely many modes that may exist for a given spatial wavelength. However, in general, only the mode that grows the fastest is of interest, as it is this mode that will come to dominate the solution over time. The

exponential coefficient in the above equation is often written as $\mu = \exp(\sigma T)$, where μ is termed the Floquet multiplier. If $|\mu| > 1$, the corresponding perturbation field grows exponentially from one period to the next and hence the base flow is linearly unstable to perturbations of the selected spatial wavelength in the z-direction.

To implement this scheme numerically, the following steps are taken. The initial perturbation field is taken to consist of random noise, for a selected spanwise wavelength. From these initial conditions, the perturbation equations are integrated forward in parallel with the base-flow equations. The spatial discretization and time-integration schemes used for this study were the same as those employed for the base-flow calculations. To obtain a measure of the Floquet multiplier μ, the L_2 norm of a perturbation field (any of the fields will suffice) is taken, and the perturbation field is then normalized by this value. The base-flow and perturbation equations are then integrated forward one base-flow period T, the L_2 norm evaluated again and the perturbation field again renormalized. The L_2 norm is the ratio of the perturbation-solution magnitudes for one period and the next. After many base-flow periods, only the fastest growing (or slowest decaying) Floquet mode remains and, at this stage, the L_2 norm corresponds to the magnitude of the largest Floquet multiplier for the selected wavelength. For this study, convergence to three significant figures was obtained within from 10 to 60 base-flow periods.

This method works very effectively for Floquet modes that have the same period as the base flow, or a period that is a multiple of the base flow (i.e. subharmonic modes). However, modes can exist that have periods incommensurate with the base flow periods. These are called quasi-periodic modes and have been found to occur in the wakes of some bluff bodies and other fluid flows (see for instance Blackburn & Lopez 2003; Marques, Lopez & Blackburn 2004; Blackburn *et al.* 2005). For these modes, the true Floquet multiplier will be a complex quantity and its imaginary component is not directly resolved by the method described above. However, this imaginary component causes an underlying sinusoidal time variation in the perturbation field, and hence the L_2 norm will also oscillate in time. Therefore, with inspection of the history of the returned Floquet multiplier and careful inspection of the perturbation fields, the existence of quasi-periodic modes can be deduced. It was also shown by Blackburn & Lopez (2003) that the magnitude of the complex Floquet multiplier is the mean value over time of the quantity returned using the L_2-norm 'power' method employed for this study.

2.3. *Discerning the critical values*

To discern where the Floquet modes become critical, the above method is applied over a range of wavelengths and Reynolds numbers, and $|\mu|$ is calculated. For each Reynolds number the multipliers must vary quadratically about each local maximum. After identifying the approximate location of any peaks of these curves, a parabolic fit can be used to determine the coordinates of each local maximum. Next, these points, for a range of Reynolds numbers, are used to determine the $|\mu| = 1$ crossing. In this way, the critical values of Re and λ can be found. For this study, steps $\Delta Re = 5$ and a maximum $\Delta\lambda = 0.1$ were employed. This process was repeated for each value of A^*. For this study λ is a non-dimensional quantity, the wavelength being normalized by the cylinder diameter.

3. Definition of the problem studied

The focus of this study is to determine the effect of the oscillation amplitude on the stability of a cylinder wake, for the case where the wake and the applied oscillation

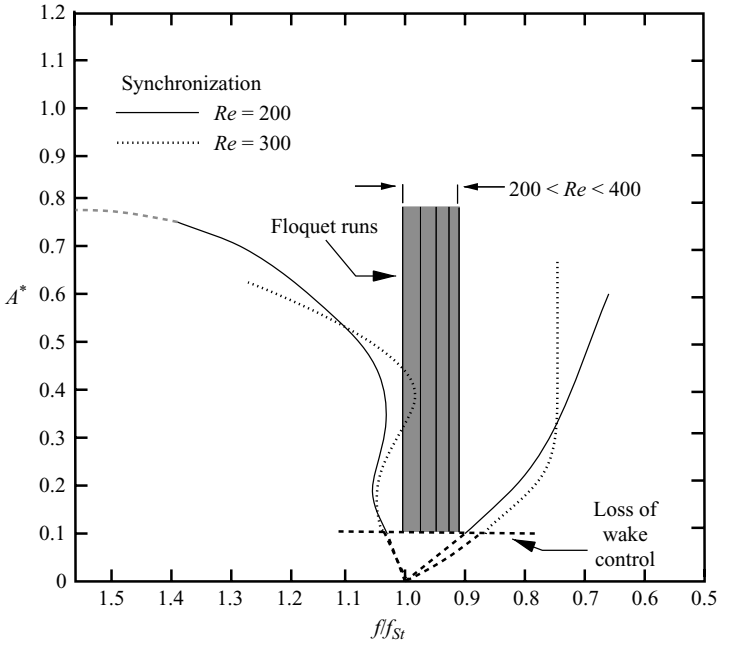

FIGURE 2. Synchronization boundaries for $Re = 200$ and $Re = 300$. The shaded box shows the region covered by the Floquet simulations, and the solid lines in this box mark increments in the Reynolds number $\Delta Re = 50$. The reason that f/f_{St} varies with Re is that f_{St} increases nonlinearly with increasing Re. It can be seen that all the simulations fall inside the synchronization region.

are locked. To reduce the complexity of the problem slightly, the non-dimensional frequency, $f^* = fU/D$, where f is the frequency of oscillation, was held fixed at 0.20 for all simulations. This value was chosen because it is close to the middle of the range of the Strouhal number for a fixed cylinder, over the range of Reynolds numbers where transition occurs. According to the three-term fit given by Williamson & Brown (1998), over the Reynolds-number range $180 < Re < 350$, the Strouhal number St spans the range $0.193 < St < 0.215$. Therefore, the value $f^* = 0.20$ is shown to be close to the fixed-cylinder Strouhal number for all the simulations conducted.

Keeping the oscillation frequency close to the fixed-cylinder Strouhal frequency ensures that the wake is synchronized with the cylinder oscillation, or 'locked-on'. This means that the wake is changed from its natural frequency to match the frequency of oscillation of the cylinder. This synchronization occurs over a wider range of frequencies as the amplitude is increased (Leontini *et al.* 2006; Williamson & Govardhan 2004). However, at amplitudes where $A^* < 0.1$ synchronization does not occur and the wake is not periodic, both the oscillation and Strouhal frequencies being present. Since Floquet stability analysis requires a periodic base flow, no stability results are shown for amplitudes $A^* < 0.1$ (except for $A^* = 0$, where the results correspond to a fixed cylinder that is shedding at the natural Strouhal frequency).

Figure 2 shows synchronization boundaries in the (A^*, f/f_{St})-plane, where f_{St} is the Strouhal frequency, along with an indication of the region where the simulations for this study fall. It can be seen that all the simulations performed for the Floquet analysis fall inside the synchronization boundaries. The fact that f/f_{St} varies, even

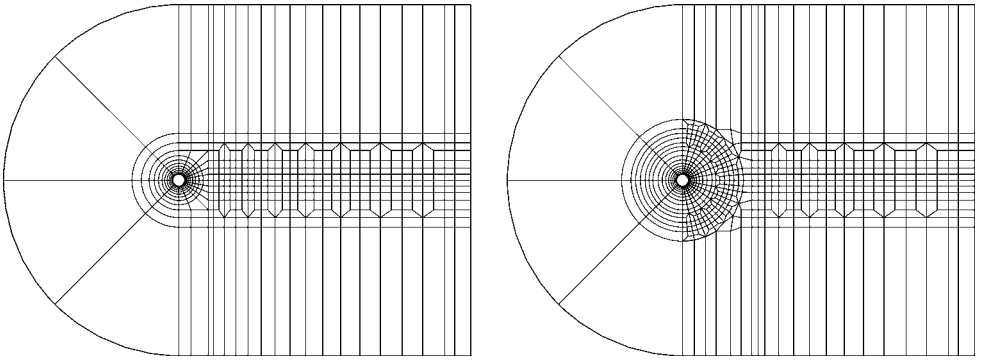

FIGURE 3. The macro-element meshes employed throughout this study. The mesh on the right was employed for simulations where $A^* \geqslant 0.7$.

though f was held constant, is due to the nonlinear increase in f_{St} with increasing Re.

4. Validation

Two spectral-element meshes were employed for this study. These meshes are illustrated in figure 3. The first has previously been shown to resolve accurately the base flow (Leontini *et al.* 2006). The second mesh shown, which has more elements in the wake region, was used at higher amplitudes of oscillation, where the wake becomes very wide. The extra resolution further away from the cylinder was required to resolve accurately the finer structures present in the perturbation field. Care was taken during the construction of this mesh to ensure adequate resolution. This was then further checked by varying the order of the interpolating polynomials of the spectral elements. It was found that increasing the polynomial order from $p = 8$ to $p = 10$ changed the value of the Floquet multiplier returned by less than 0.1%. From this result, it was concluded that the meshes employed, using a tensor product of eighth-order polynomials within elements, provided sufficient resolution to resolve accurately the finer-scale structures associated with the Floquet modes.

The methods employed throughout this study have been used previously and shown to give accurate results (Sheard *et al.* 2003; Ryan *et al.* 2005; Thompson 2006). However, a validation study was conducted to ensure that the current implementation produced results in agreement with standard test cases. The natural case against which to validate was that of a fixed cylinder. The modes present and the critical values of λ and Re are well established, and the basic structures of the modes are available in the literature.

Simulations were run for $Re = 190$, and the stability of a mode with $\lambda = 4.0$ was tested; these values are very close to the critical values for mode A reported by Barkley & Henderson (1996), which were $Re = 188.5$ and $\lambda = 3.96$. A Floquet multiplier $\mu = 1.0155$ was calculated, indicating that the mode was only just supercritical, as expected.

Similarly, simulations were run for $Re = 260$, and a mode with $\lambda = 0.8$ was tested for stability. The critical values for mode B are $Re = 259$ and $\lambda = 0.822$ (Barkley & Henderson 1996). Using these almost-critical values, a Floquet multiplier $\mu = 1.0336$ was obtained, confirming that the method employed also correctly resolved this finer-scale mode.

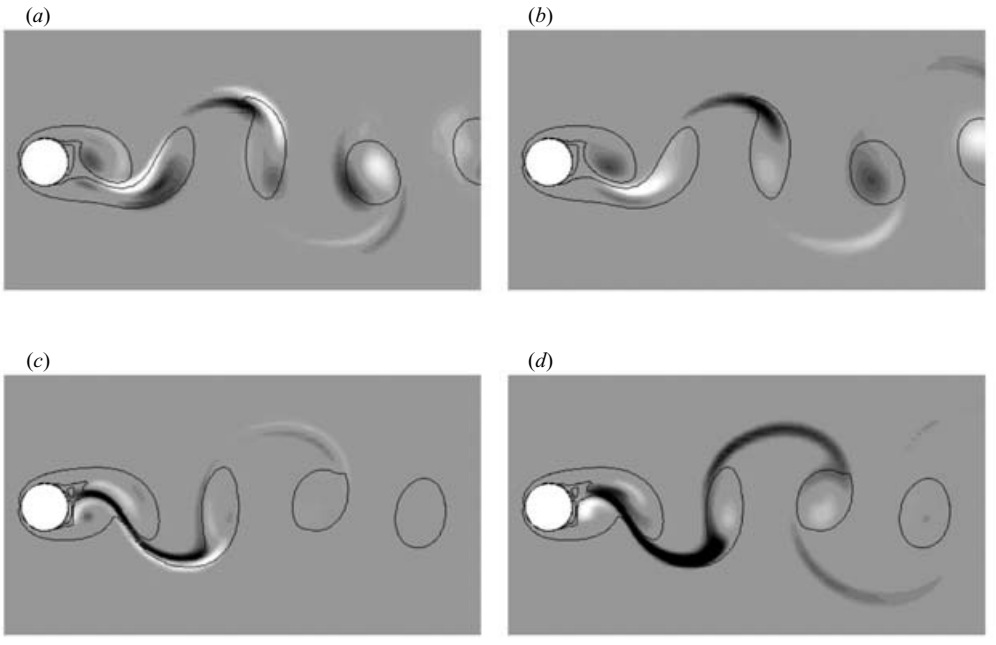

FIGURE 4. (*a*) Spanwise and (*b*) streamwise vorticity for mode A in the wake of a fixed cylinder; $Re = 190$, $\lambda = 4.0$. The mode has just become unstable. (*c*) Spanwise and (*d*) streamwise vorticity for mode B in the wake of a fixed cylinder; $Re = 260$, $\lambda = 0.80$. Again, the mode has just become unstable. These results are very close to those in figures 10 and 11 in Barkley & Henderson (1996).

Further confirmation of the ability to resolve mode-A- and mode-B-type structures is found in figure 4. This figure shows the spanwise and streamwise perturbation vorticity fields for both the validation cases outlined here. These plots compare favourably with those obtained by previous researchers (Barkley & Henderson 1996; Ryan *et al.* 2005).

To ensure that the method could also predict accurate critical values for quasi-periodic modes, simulations were run to establish the critical Re and λ values for mode QP for a fixed-cylinder wake. While the method used does not automatically return the total complex Floquet multiplier, it has been shown that the magnitude of μ is equal to the mean value returned over a number of base-flow periods (Blackburn & Lopez 2003). Using this method, Floquet runs were performed over a wavelength range $1.5 \leqslant \lambda \leqslant 2.0$, and a Reynolds number range $370 \leqslant Re \leqslant 380$. From these results, the critical Re for mode QP was estimated to be about 377 and the critical λ to be about 1.8. These values are the same as those reported by Blackburn *et al.* (2005). It was therefore concluded that if care is taken in the interpretation of results, the method utilized can resolve quasi-periodic modes and distinguish them from true subharmonic modes.

5. Results

5.1. *Wake modes and three-dimensional transitions*

In the case of a fixed cylinder, only one variable, Re, governs the wake behaviour. Stability and bifurcation analyses therefore proceed by slowly varying Re and assessing

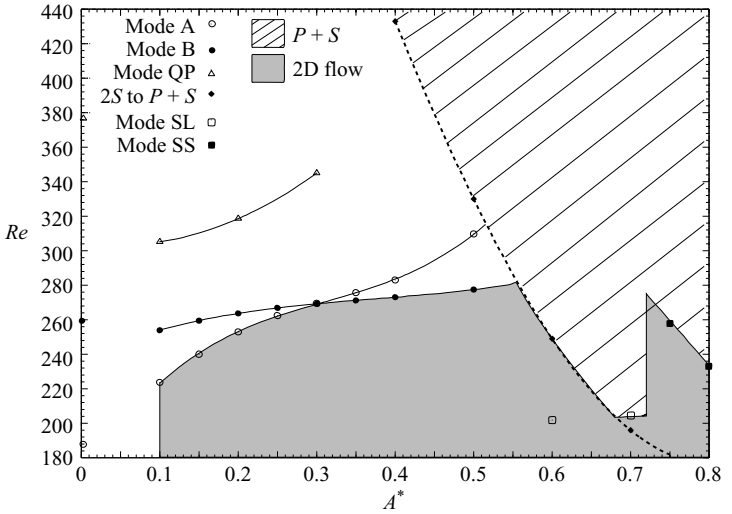

FIGURE 5. A transition diagram, showing the curves of criticality for mode A, mode B, mode QP, mode SL and mode SS as a function of A^*. Also shown, by a line of dots, is the boundary defining the transition from a $2S$ to a $P+S$ wake configuration. The shaded grey area indicates that the flow is two-dimensional. The hatched area denotes where the $P + S$ base flow is present.

when the two-dimensional base flow becomes unstable to the three-dimensional modes. However, in the case of the oscillating cylinder a second variable exists, the amplitude of oscillation. Therefore, instead of there existing a single critical value of Re for a given mode, the critical Re is now a function of A^*. To determine the functional variation, the critical Re for a given mode was first found for a set value of A^*. The latter was then incremented, and the critical Re again found. This process was repeated until the parameter space was spanned. By performing the analysis in this way, a map showing the criticality of all the modes and transitions present in the (A^*, Re)-plane can be constructed.

Such a map is presented in figure 5. This figure shows various lines defining different transitions. A line of dots dividing the plane approximately vertically defines the transition from the $2S$ to the $P + S$ wake mode. This line shows explicitly that this wake-mode transition of the base flow has an Re-dependence, the value of A^* at the transition varying inversely with Re; similar results have previously been shown implicitly for two-dimensional flow (Leontini *et al.* 2006). The transition to three-dimensional flow differs markedly for the two different base flows lying on either side of this transition.

The base flow to the left of this transition (i.e. at lower A^* values) is the $2S$ wake mode. From this base flow, three-dimensional modes are seen to bifurcate. These correspond to mode A, mode B and the quasi-periodic mode QP. These three modes share features similar to the corresponding modes in a fixed-cylinder wake. The details of each mode is provided in the subsequent sections.

At low amplitudes of oscillation, for $A^* < 0.3$, the order of criticality of the three modes is the same as for a fixed cylinder. With respect to Re, mode A becomes critical first, then mode B and finally mode QP. Increasing A^* has the effect of increasing the critical Re for all the modes. However, this effect is much more pronounced for mode A than for mode B or the other modes. The net result is that at $A^* \simeq 0.3$ the critical

Re for mode A matches that of mode B, and for $A^* > 0.3$ the order of inception of modes A and B with respect to *Re* is reversed, mode B now becoming critical before mode A.

Previous studies have also shown that, by varying a second parameter, the order of onset of the modes can change. This was observed by Ryan *et al.* (2005). As they varied the aspect ratio of elliptical leading-edge plates, the order of inception of what were called mode A and mode B′ was reversed (the prime indicates that the spatio-temporal symmetry was the same as for the mode B as described here but that features such as the critical wavelength and near-wake structure were different). However, this is the first time, to the authors' knowledge, that a 'pure' mode B has been observed to become critical before mode A, without the explicit suppression of mode A. It has been shown that if mode A is suppressed, by restricting the spanwise domain size, a nonlinear development of mode B can lead to a period-doubling cascade and thence to turbulence (Karniadakis & Triantafyllou 1992). This suggests that for an oscillating-cylinder wake the transition to turbulence may take a different route depending on the amplitude of oscillation. This same observation was made for the elliptical leading-edge plate by Thompson (2006).

For an oscillating cylinder, mode QP was found always to become critical at Reynolds numbers greater than those for both modes A and B, at least for the frequency of oscillation used here. This suggests that the mode QP plays a minimal role in experimental flows, as the flow will already be strongly three-dimensional and chaotic for the Reynolds numbers required for its positive growth. Like the fixed cylinder, this leaves modes A and B as the two most physically relevant modes.

To the right of the $2S$ to $P+S$ transition in figure 5 (at higher A^* values), the base flow is the $P+S$ wake mode. With the onset of this two-dimensional wake mode, modes A, B and QP cease to exist. Instead, two new three-dimensional modes, here called mode SL and mode SS, are present. The first character, S, indicates that the modes are true subharmonic modes and the second character, L or S, indicates long or short wavelengths, respectively.

It is reasonable to expect subharmonic modes to arise from a base flow that does not possess Z_2 symmetry. Such a modified base-flow symmetry group is known to allow true subharmonic modes, as discovered in the wake of tori by Sheard *et al.* (2003). In the case of tori, a subharmonic mode is the first to become critical with respect to *Re* for diameter ratios *Ar* in the range $4 \leqslant Ar \leqslant 8$. For the case of the oscillating cylinder presented here, the subharmonic modes are the first to reach criticality once the base flow takes on the $P+S$ configuration.

Focusing on the transition scenario where the base flow is in the $P+S$ configuration, some interesting observations can be made. First, for amplitudes where $A^* \lesssim 0.67$, mode SL is shown to grow for all *Re* where the $P+S$ wake exists. After $A^* \simeq 0.67$, there is a region where the base flow takes on the $P+S$ pattern, in which three-dimensional modes do not grow. This finding predicts that a two-dimensional $P+S$ wake is physically realizable, as has been shown by the flow visualization at low *Re* of Williamson & Govardhan (2004). However, it has also been stated (Williamson & Roshko 1988) that the $P+S$ wake mode is not observed (until much higher A^*) at $Re > 300$ in experiments, where the flow has, until now, been assumed to be three-dimensional. Therefore, if mode SL relies on the $P+S$ wake mode to materialise, it is unlikely that it will be observed in a physical experiment even though it may instigate the breakdown to three-dimensionality. It seems that the path to turbulence in which mode SL is the first three-dimensional transition will be very complex.

A^* range	Mode inception order (with increasing Re)
$A^* < 0.3$	A, B, QP
$0.3 < A^* < 0.55$	B, A
$0.55 \lesssim A^* \lesssim 0.67$	(P + S), SL
$0.67 \lesssim A^* \lesssim 0.72$	P + S, SL
$A^* > 0.72$	P + S, SS

TABLE 1. Mode inception order with increasing Re for successive ranges of A^*. For the ranges indicated, four different three-dimensional modes occur first. The parentheses around P + S denote that in the corresponding range the P + S two-dimensional mode is inherently unstable to three-dimensional perturbations.

Second, the two-dimensional $P+S$ wake mode is observed to be inherently unstable to mode SL for $0.55 \lesssim A^* \lesssim 0.67$. As the Re value at the $2S$ to $P+S$ transition varies inversely with A^*, this effectively means that the Re value at the transition to three-dimensionality also varies inversely with A^*. This is an important finding, as it had been thought that the oscillation of the cylinder would delay the onset of three-dimensionality; yet here, for a range of A^*, the opposite is predicted to occur.

For amplitudes where $0.67 \lesssim A^* \lesssim 0.72$, there is a small region for low Reynolds numbers where the $P+S$ mode exists without mode SL growing. For this range, mode SL is still the first three-dimensional mode to become critical. Increasing the amplitude further, beyond $A^* \gtrsim 0.72$, has the result that mode SL will never become critical. This phenomenon is elaborated on in § 5.7. The 'dying-out' of mode SL leaves mode SS as the first three-dimensional transition, and hence there is a sudden jump in the critical Re. Further increases in A^* sees the critical Re drop again.

How the behaviour of these subharmonic modes will be manifested physically is yet to be seen. The fact that the $P+S$ wake mode is not observed once the flow is three-dimensional suggests that there is a complex nonlinear interaction between the Floquet mode and the two-dimensional base flow, to the point where the unstable three-dimensional mode modifies the two-dimensional topology that it depends upon for growth. There may be strong hysteretic effects present. In short, while the findings of this linear stability analysis are very interesting and novel, it seems that three-dimensional simulations or carefully controlled experiments are required to complete the picture for the wake flow in this region of the parameter space.

However, the linear analysis clearly renders some interesting points that can be used to guide such an investigation. One such point is that, for the oscillating cylinder, there are four different three-dimensional modes that become critical first, over successive ranges of A^*. Mode A is the leading three-dimensional mode for $A^* < 0.3$ and mode B for $0.3 < A^* < 0.55$. Following the transition to the $P+S$ wake mode, mode SL is the first to become critical for $0.55 < A^* < 0.72$, and finally mode SS for $A^* > 0.72$. The order of inception of the different modes is summarized in table 1. This variation in the leading mode suggests that multiple routes to turbulence may be possible in the wake of an oscillating cylinder, depending on A^*.

In the following sections, details of each of the three-dimensional modes are presented. These include the symmetries, similarities and differences in the modes when compared with those of other bluff-body wakes and also some discussion of their physical causes and instability types.

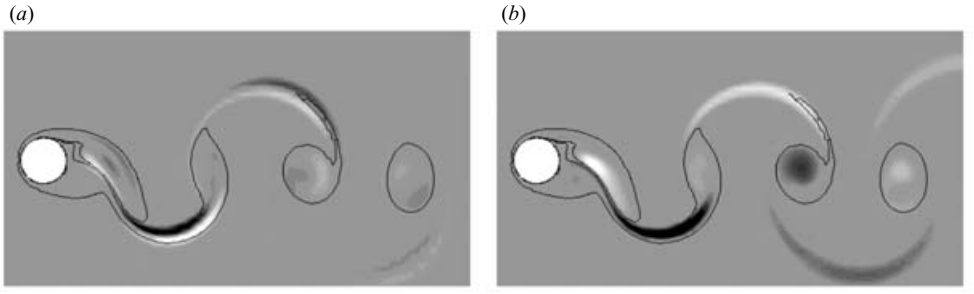

FIGURE 6. (*a*) Spanwise perturbation vorticity for mode A, where $A^* = 0.3$, $Re = 280$, and $\lambda = 2.8$. This pattern is very similar to that for mode A for a fixed cylinder. (*b*) Streamwise perturbation vorticity for the same conditions. The spatio-temporal symmetry is the same as that for mode A for a fixed cylinder.

5.2. *Mode A*

The mode-A instability of an oscillating cylinder is very similar in character to that for a fixed cylinder. In particular, mode A retains the spatio-temporal symmetry of the base flow (in terms of the velocity field). Mode A still appears to be an instability of the primary vortex cores. This, along with the symmetry of the mode, is confirmed by an inspection of figure 6, which shows the perturbation-field streamwise and spanwise vorticities for mode A at $A^* = 0.3$, $Re = 280$ and $\lambda = 2.8D$, the latter being close to the fastest growing wavelength. The spanwise vorticity shows that the forming primary vortex at the rear of the cylinder contains both positive and negative regions of perturbation vorticity, and then a high amplitude of the perturbation field in the high-strain region between vortices. Further downstream, the perturbation is most concentrated in the primary vortex cores. This perturbation field is very similar to that for the wake of a fixed cylinder, as shown by Thompson *et al.* (2001). In their case, the perturbation-field arrangement was interpreted as consisting of a cooperative elliptic instability close to the rear of the cylinder and a downstream elliptic instability in the shed-vortex cores. The results here suggest the same mechanisms apply to mode A for the oscillating cylinder. The streamwise perturbation vorticity further highlights the spatio-temporal symmetry of mode A, the streamwise vorticity changing sign every half-period (which corresponds to the reflection of the velocity field, and therefore a change in sign of the y-component of velocity, on opposite sides of the wake).

Increasing the amplitude of oscillation also affects the fastest growing wavelength of mode A. The fastest growing wavelength at the critical Re versus the amplitude of oscillation is plotted in figure 7. What is shown is that the critical λ decreases as A^* increases. This decrease is almost linear. One possible explanation is that as the amplitude increases, the vortices shed into the wake become increasingly compact, effectively reducing the diameter of the vortex cores. As the mode-A wavelength presumably scales with the vortex-core diameter (Leweke & Williamson 1998), this wavelength is reduced for the narrower cores. This narrowing of the shed-vortex cores is shown in figure 8. Vorticity plots of the base flow close to where mode A becomes critical are shown for $A^* = 0.1$ and $A^* = 0.5$. It is clear that the vortices are much more highly strained, and narrower, for the higher amplitude of oscillation. In fact, the negative vortex about to be shed when $A^* = 0.5$ is approximately 0.69 the width of the same vortex when $A^* = 0.1$. The critical λ when $A^* = 0.5$ is approximately 0.73 times that at $A^* = 0.1$. An agreement such as this is not conclusive but is consistent with such a hypothesis for the linear decrease in λ.

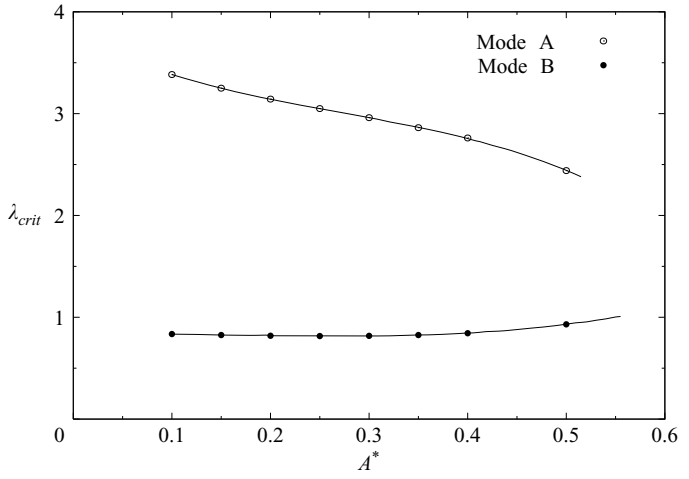

FIGURE 7. Fastest-growing wavelength for modes A and B at criticality plotted against A^*. Mode A has its wavelength shortened by an increase in amplitude, whereas the mode-B wavelength is almost unchanged.

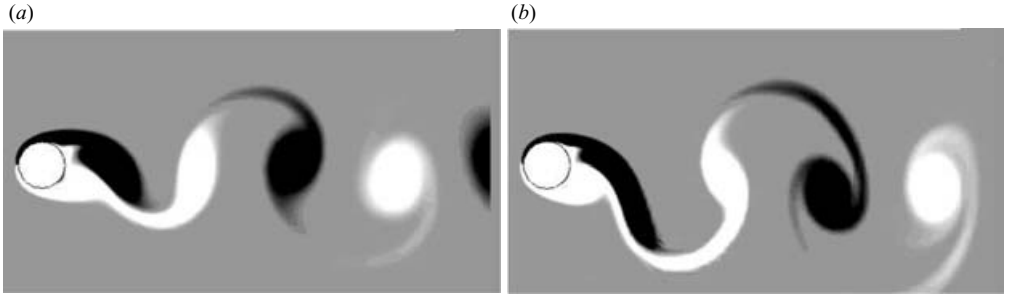

FIGURE 8. The base-flow vorticity when mode A becomes critical for (*a*) $A^* = 0.1$ and (*b*) $A^* = 0.5$. It is clear that the shed vortices narrow with increasing A^*.

The elliptic instability theory developed by Landman & Saffman (1987) has been applied to fixed-cylinder wakes by Leweke & Williamson (1998) and Thompson *et al.* (2001) and predicts a fastest growing wavelength for mode A of $\simeq 3D$. From Leweke & Williamson (1998), the fastest growing wavelength can be predicted using the formula

$$\lambda = D\left(\frac{2}{1-\beta}\right)^{1/2} \tan\theta, \tag{5.1}$$

where β is the eccentricity parameter at the centre of the vortex and θ is the angle of the wave vector to the z-axis. Values of θ were found from the numerical results presented in Landman & Saffman (1987). For validation, the method was employed on the wake of a fixed cylinder at $Re = 190$ and a wavelength $\lambda = 2.9D$ was recovered, in close agreement with the value $\sim 3D$ found in Leweke & Williamson (1998).

The results for the wavelength prediction for the oscillating cylinder at a series of amplitudes are shown in figure 9. It is shown that the theory predicts shorter wavelengths for the oscillating cylinder than for the fixed cylinder. It also predicts that, on the whole, the critical wavelength should decrease with increasing amplitude,

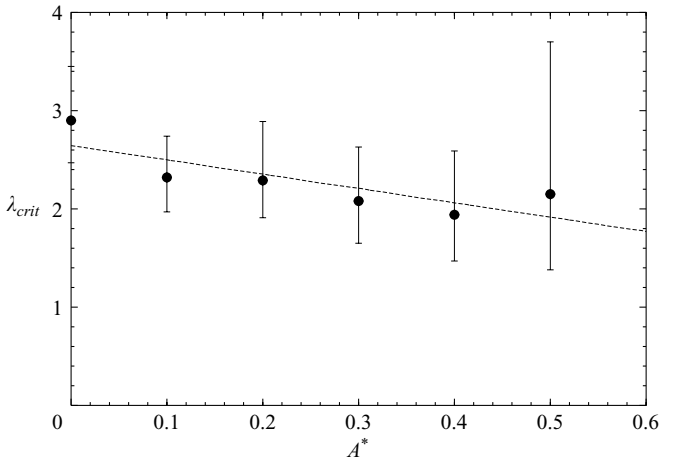

FIGURE 9. Critical-wavelength variation with amplitude, as predicted by elliptic instability theory. The theory predicts shorter wavelengths as the oscillation amplitude is increased.

as indicated by the least-squares line fit and accords with the Floquet analysis, as seen in figure 7.

The predicted wavelength at $A^* = 0.5$ seems to break the trend of decreasing critical λ with increasing A^*. However, it should be noted that as the eccentricity becomes high (i.e. where the vortices become more elliptical), the predicted wavelength becomes very sensitive to the value of β, as is clear from inspection of (5.1). For $A^* = 0.5$, the value of β calculated was $\beta = 0.95$, near the upper limit, $\beta = 1$, for elliptical flow. This accounts for the large error bars at this point. The error bars at all points were estimated by assuming an accuracy of ± 0.025 for the eccentricity β and an accuracy of $\pm\pi/48$ for θ. Even so, the overall trend of the theory shows a reduced wavelength with increasing amplitude, which is consistent with the Floquet analysis. This is further evidence that mode A is (primarily) caused by an elliptic instability (Leweke & Williamson 1998; Thompson *et al.* 2001).

5.3. *Mode B*

As with the mode-A instability, mode B was found to be analogous in structure to mode B for a fixed cylinder. The symmetry of the mode is the same in both cases, the streamwise vorticity repeating every half base-period rather than every period as occurs for mode A. This results in what appears to be a continuous tube of streamwise vorticity being formed that connects the successive, but opposite-signed, base-flow vortices. A plot of the streamwise vorticity is shown in figure 10. This clearly shows a connecting 'tube' of vorticity between the base-flow vortices.

Also shown in figure 10 is a plot of the spanwise perturbation vorticity for mode B. Leweke & Williamson (1998) presented results which indicated that mode B for a fixed cylinder was a hyperbolic instability of the braid shear layers between the primary vortices, partly due to the high amplitude of the instability in these regions. Evidence was also presented by Ryan *et al.* (2005) that a centrifugal instability plays a role. Comparison of the spanwise perturbation vorticity presented in figure 10 with that for mode B of a fixed cylinder (Barkley & Henderson 1996; Ryan *et al.* 2005) shows that the two are very similar. It is therefore proposed that the same mechanism causes mode B for an oscillating cylinder as for a fixed cylinder.

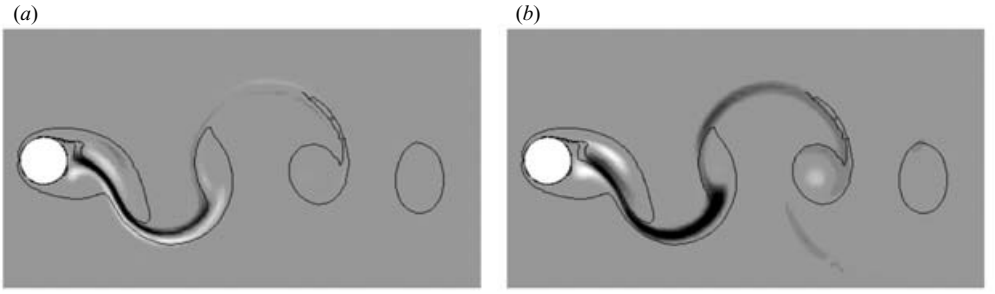

FIGURE 10. (*a*) Spanwise perturbation vorticity for mode B, where $A^* = 0.3$, $Re = 280$ and $\lambda = 0.85$. This pattern is very similar to that for mode B for a fixed cylinder. (*b*) Streamwise perturbation vorticity for the same conditions. The spatio-temporal symmetry is the same as mode B for the fixed cylinder.

Unlike mode A, the critical wavelength of mode B is hardly affected by the oscillation amplitude, maintaining a nearly constant value of $\lambda \simeq 0.8$. This effect is illustrated by plotting the fastest-growing wavelength for mode B at criticality versus the amplitude of oscillation as in figure 7. Interestingly, Sheard *et al.* (2003) also observed an almost constant value for the fastest growing mode-B wavelength in the wake of various different tori. The issue of mode-B wavelength selection is still under investigation.

5.4. *Mode QP*

Mode QP is influenced by the amplitude of oscillation in two different ways, as can be deduced from an inspection of figure 5. It had previously been established that mode QP for a fixed cylinder becomes critical at $Re \simeq 377$ (Blackburn *et al.* 2005). This result is confirmed by the validation study reported in § 4.

The first effect of the oscillation is to reduce this critical Re quite significantly, to $Re \simeq 305$ for an amplitude of oscillation $A^* = 0.1$, which is close to the lowest amplitude at which synchronization of the base wake flow and the cylinder oscillation can be obtained (Koopman 1967). However, this trend is not continued as A^* is increased further. For $A^* > 0.1$, increasing the amplitude of oscillation causes the critical Re for mode QP increase, to until it reaches $Re \simeq 345$ for $A^* = 0.3$. Note that the sudden drop in the critical Reynolds number from $A^* = 0$ to $A^* = 0.1$ may be due to the shift in wake frequency from the natural Strouhal shedding frequency of the two-dimensional base flow to the applied frequency, $f = 0.2$.

At amplitudes higher than $A^* \geqslant 0.3$, the critical values of Re and λ for mode QP become harder to determine, because the method currently employed to detect the Floquet modes returns only the fastest growing mode and, at these higher amplitudes, mode A becomes the fastest growing mode at increasingly shorter wavelengths, which intrudes on the range of wavelengths that mode QP covers. This is illustrated in figure 11. Plotted is the magnitude of the Floquet multiplier for the fastest growing mode over a range of wavelengths that encompasses modes A, B and QP. The amplitude and Reynolds number are fixed at $A^* = 0.3$ and $Re = 350$, respectively. It is shown that the data points representing mode QP have no turning point – no peak that can be identified for the fastest growing wavelength. It should be noted that the point presented as critical at $A^* = 0.3$ in figure 5 was obtained by extrapolating a quadratic function fitted to the data with a least-squares method.

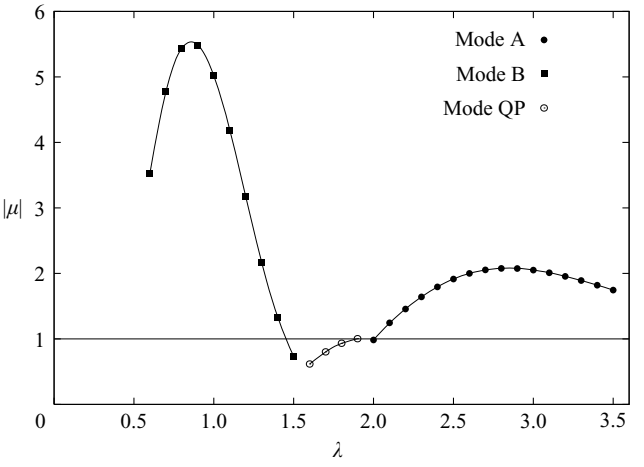

FIGURE 11. Floquet multiplier vs. wavelength when $A^* = 0.3$, $Re = 350$. Mode QP is just becoming critical, but the growth rates of both mode A and mode B are much higher. The range of wavelengths covered by mode A encroaches on that of mode QP, meaning that no turning point can be defined with interpolation.

Figure 11 also shows that while mode QP is close to critical for these conditions, mode B and mode A both have far higher growth rates, which suggests again that it is these two modes that are physically the most relevant.

The existence of mode QP was deduced from the oscillation in the growth rate and observation of the perturbation fields. The magnitude of the complex Floquet multiplier was deduced by taking the mean value over the period of oscillation of the Floquet multiplier (Blackburn & Lopez 2003).

Shown in figure 12 is a series of images of the perturbation field taken one base-flow period apart, for $A^* = 0.3$ and $Re = 350$. The series of images spans approximately one period of oscillation of the Floquet multiplier. It is seen that the perturbation field almost repeats over two base periods. That it is not quite periodic is manifested by the gradual growth and decay of the perturbation field on a much longer time scale.

This is highlighted, for instance, by focusing on the initially positive region (shown in white) of perturbation vorticity inside the vortex at the immediate rear of the cylinder in the first image. Scanning down the page, comparing images two base periods apart, shows that this region gradually weakens and eventually changes sign. This illustrates that the mode is truly quasi-periodic and as such it repeats with a period incommensurate with the base flow.

As the mode is quasi-periodic, the Floquet multiplier is seen to oscillate over time when it is calculated as the growth rate from one base flow period to the next. While noting that the period of this oscillation is directly related to the period of the three-dimensional mode, the associated frequencies are not reported in this paper.

This period was found to be relatively stable with respect to the amplitude of oscillation and Re, but it varies considerably over a band of wavelengths. This is illustrated in figure 13. The time history for a series of wavelengths is plotted for $A^* = 0.3$ and $Re = 350$. It is clear that the period of oscillation is increasing with increasing wavelength. This variation makes it difficult to hypothesise about the possible physical mechanisms behind this instability, owing to the fact that the maximum occurs at different places at different times.

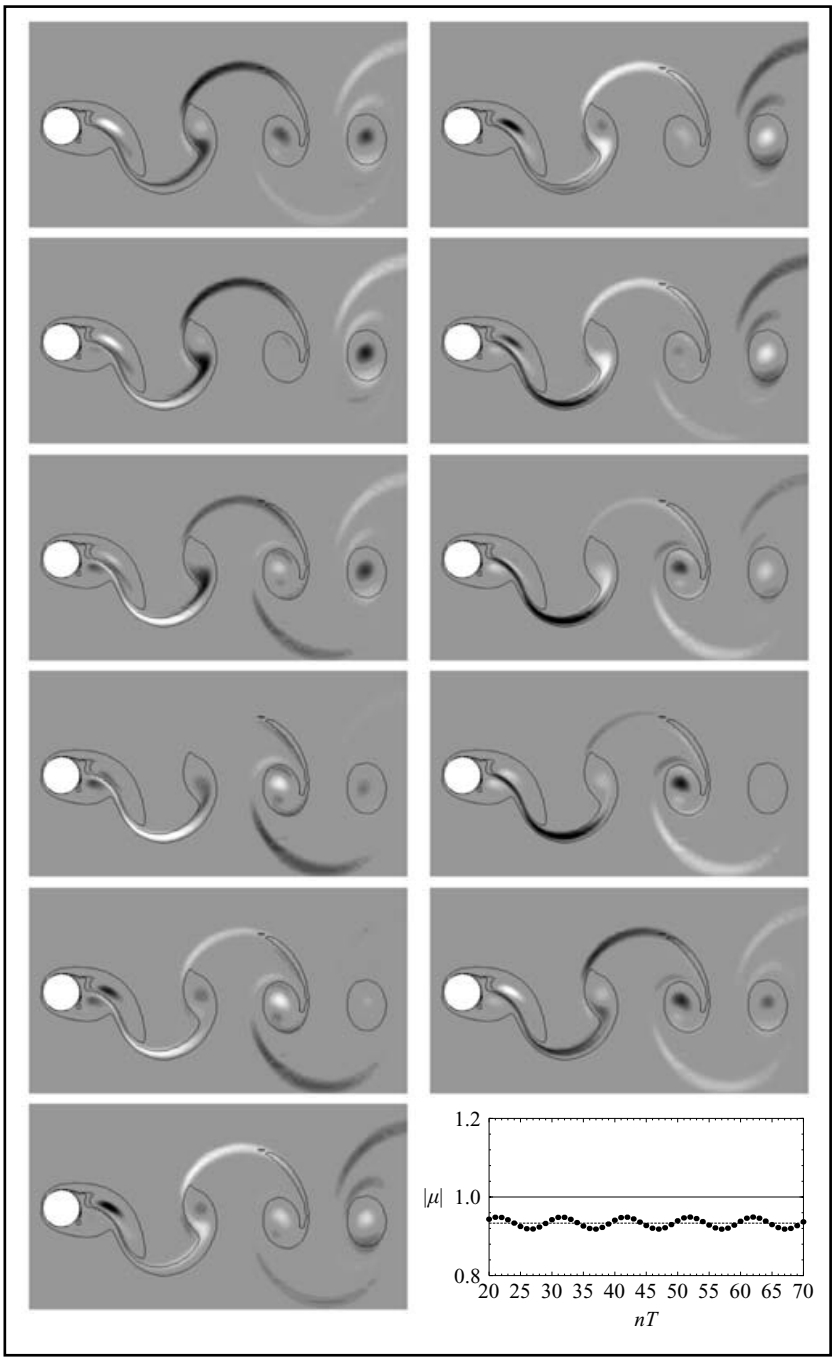

FIGURE 12. Streamwise vorticity of the quasi-periodic mode, when $A^* = 0.3$, $Re = 350$ and $\lambda = 1.8$. Images are set at one base-flow period apart and should be read left to right, top to bottom. It is seen that the mode almost repeats every two base periods, except for the growth and decay of the modes in the free-shear layers connecting the base-flow vortices. The plot in the bottom right-hand corner shows the oscillation in the Floquet multiplier over time. The series of images covers approximately one period of this oscillation.

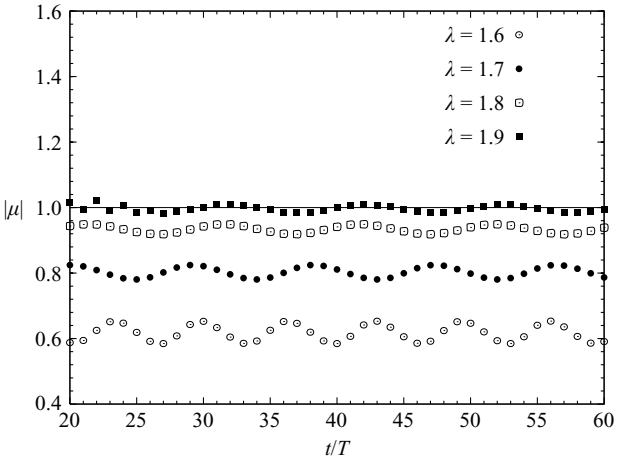

FIGURE 13. History of the Floquet multiplier for the quasi-periodic mode, when $A^* = 0.3$ and $Re = 350$. The period of the oscillation becomes longer with increasing λ, until at $\lambda \simeq 1.9$, it appears that the oscillation has almost disappeared.

5.5. *Mode SL: the first subharmonic mode*

The first subharmonic mode detected after the transition to the $P + S$ shedding mode has been called mode SL. Here, the 'S' designates as the mode subharmonic and the L indicates that this mode has a longer wavelength than the second subharmonic mode, to be discussed later. An example of the spanwise perturbation vorticity of this mode is shown in figure 14. Four images are shown, taken at half-period intervals (the cylinder is at its zero displacement position in each image). As well as illustrating where the mode grows, the subharmonic nature of the mode is highlighted by comparing the images that are separated by a full period, i.e., by comparing the top images and the bottom images. It is seen that over one period the structure of the mode is the same except for a sign change of the perturbation field.

Inspection of figure 14 shows that the mode originates in the region between the forming vortices in the near wake. However, this does not happen every half-cycle, but instead occurs only in the half during which the strong vortex of the pair of vortices in the $P + S$ wake (the vortex that does not split) is shed. This coincides with the 'up'-stroke in the images of figure 14 and is demonstrated by the high levels of perturbation vorticity in the leftmost images in this figure. As this vortex proceeds to roll up and is shed into the wake, the perturbation is transferred to the vortex core, as demonstrated by the perturbation vorticity in the rightmost images of figure 14. After this, the mode appears to be quickly dissipated downstream.

A true subharmonic was found in the wake of tori by Sheard *et al.* (2003); it was later demonstrated to lead to a period-doubling bifurcation, in Sheard *et al.* (2005). While even the two-dimensional wake topology is different in the ring wake and the oscillating cylinder, comparison of the perturbation fields seems to indicate that mode C in the wake of the torus and mode SL in the wake of the oscillating cylinder are similar in some respects. However, this similarity is not enough to deduce that they are attributable to the same or similar physical mechanisms, at this stage. This is so despite a fairly close agreement in the fastest growing wavelength of the two modes: mode C in the torus wake grows fastest at around $\lambda = 1.6$ and mode SL described here grows fastest at around $\lambda = 1.4$.

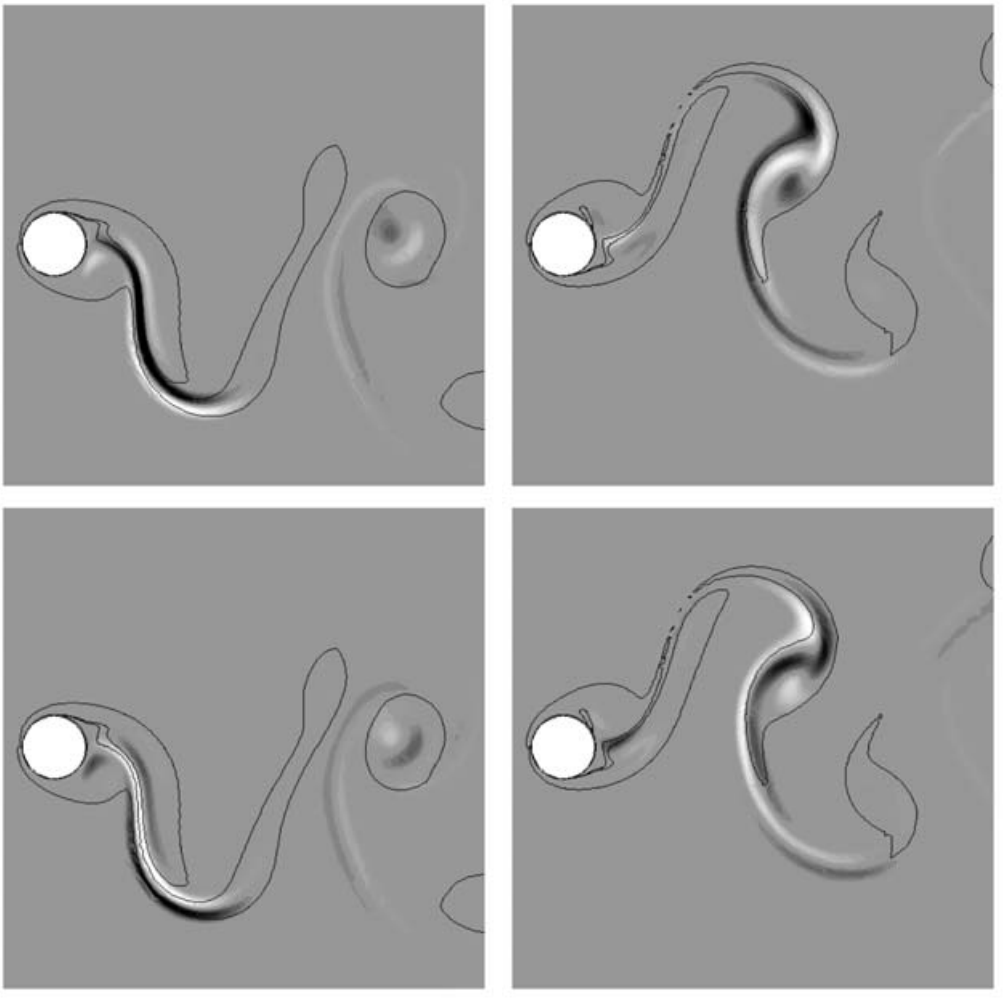

FIGURE 14. Spanwise perturbation vorticity for mode SL, when $A^* = 0.70$, $Re = 205$ and $\lambda = 1.4$. The images are taken half a period apart and should be read left to right.

5.6. *Mode SS: the second subharmonic mode*

The second subharmonic mode has been called mode SS. Here, the first 'S' designates the mode as subharmonic and the second 'S' signifies that the mode has a shorter wavelength than mode SL, discussed previously. Its near-wake structure, in terms of the perturbation spanwise vorticity, is shown in figure 15. The spanwise vorticity clearly shows where the mode is at its strongest. Again, the subharmonic nature of the mode is illustrated by comparing the top images and the bottom images and observing that over one period the mode structure is the same except for a change in sign.

Figure 15 also shows that mode SS appears to originate in the forming stronger vortex of the pair of vortices in the $P + S$ configuration (the vortex that does not split), during the up-stroke of the examples shown in figure 15. However, the mode does not stay focused in this vortex. It is stretched out and transferred to the forming vortex of the next half-cycle (the vortex that does split), during the "down"-stroke.

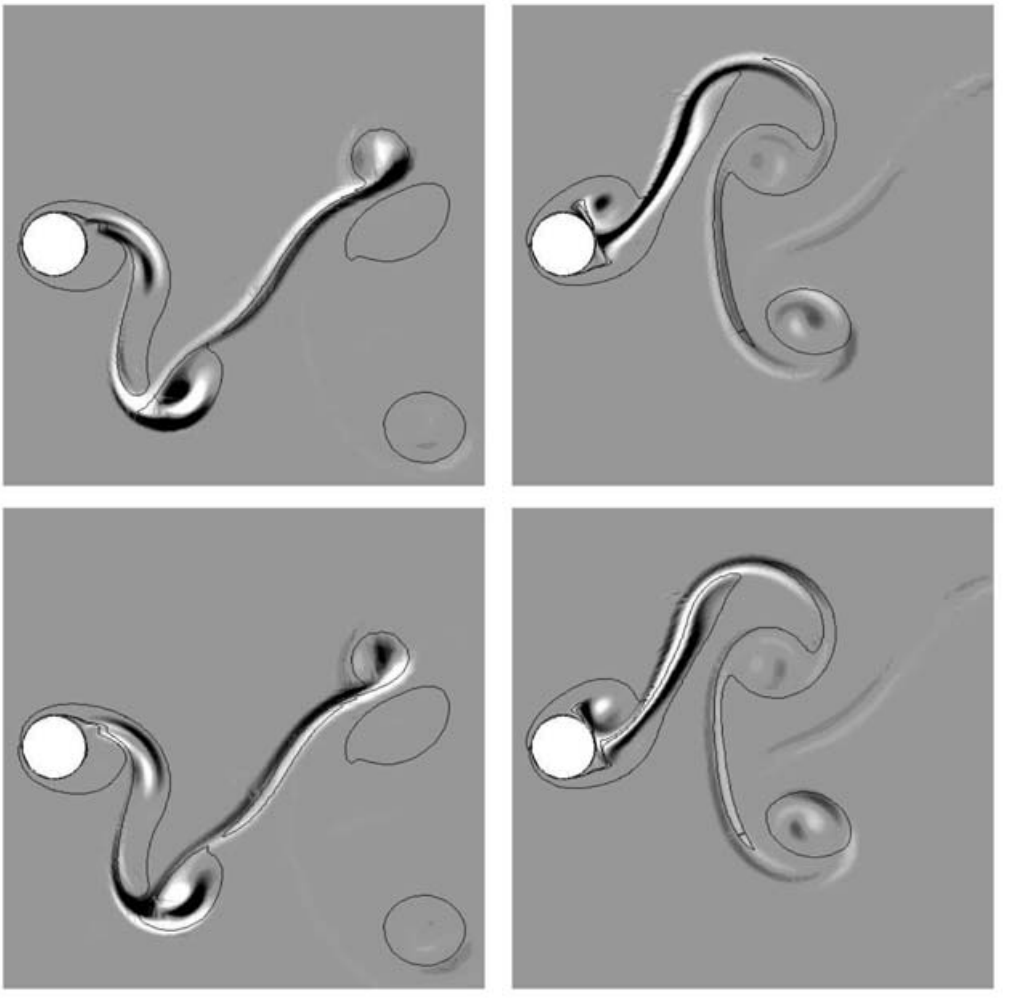

FIGURE 15. Spanwise perturbation vorticity for mode SS when $A^* = 0.75$, $Re = 260$ and $\lambda = 0.70$. The images are half a period apart, reading left to right.

During the splitting process, the vortex becomes highly strained and very narrow. It is in this region of the flow that the mode is strongest, as can be deducd from the high levels of perturbation vorticity in this region in all the images of figure 15.

This is a distinguishing feature between the two subharmonic modes, mode SL and mode SS. Mode SL is supported primarily by the vortex that does not split, whereas mode SS is supported by the vortex that does split. The critical wavelength of mode SS is quite short, around $\lambda = 0.75$. This wavelength could be linked with the very narrow, highly strained, vortex structure of this splitting vortex in the $P + S$ wake.

5.7. *Behaviour of the subharmonic modes with increasing* A^*

From amplitudes where the $2S$ to $P + S$ transition occurs, until $A^* \simeq 0.7$, mode SL is the first three-dimensional mode to become critical. In fact, for values of $A^* \lesssim 0.67$, mode SL is predicted to grow for all values of Re where the $P + S$ shedding mode is observed. In other words, it is predicted that, for $A^* \lesssim 0.67$, the $P + S$ shedding mode

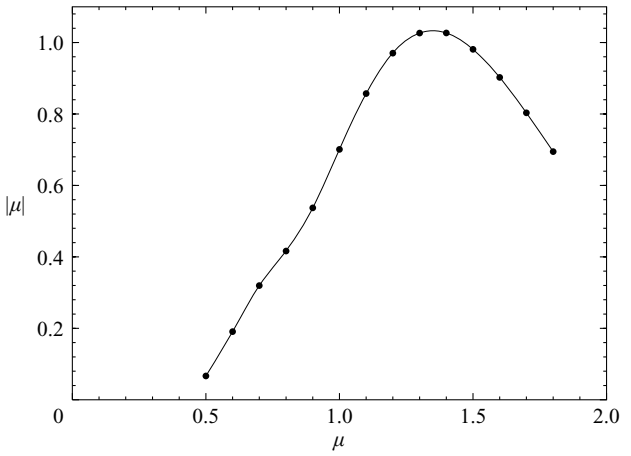

FIGURE 16. Floquet multiplier vs. wavelength when $A^* = 0.7$, $Re = 205$. One continuous curve is resolved over the range $0.5 < \lambda < 2.0$. This curve is representative of mode SL. For $\lambda > 2.0$, another quasi-periodic mode is resolved.

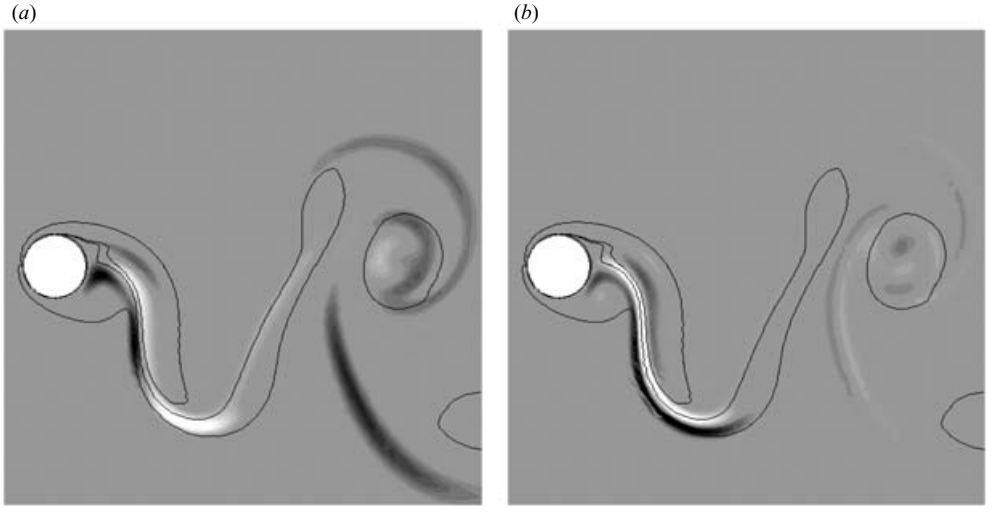

FIGURE 17. (*a*) Streamwise and (*b*) spanwise perturbation vorticity when $A^* = 0.7$, $Re = 205$ and $\lambda = 0.70$. Comparison with figures 14 and 15 shows that this is in fact mode SL.

will never be observed as a pure two-dimensional shedding mode experimentally, regardless of *Re*. It is expected that as soon as the $P + S$ mode of shedding develops, mode SL will begin to grow, introducing three-dimensionality into the flow.

Also, for $A^* \leqslant 0.7$, mode SL is the only subharmonic mode resolved using our current method, as it is faster growing than mode SS over all wavelengths tested (see § 2.2 for an explanation of how modes are resolved for a particular wavelength). This effect is highlighted in figure 16. It is shown that one continuous curve of multipliers is returned over the wavelength domain $0.5 < \lambda < 2.0$ when $A^* = 0.70$. This fact, along with careful inspection of the perturbation field at the lower wavelengths, where mode SS might be expected to be observed, confirms that mode SL is the fastest growing over this entire range of λ. An example perturbation field at $\lambda = 0.7$ is shown in figure 17.

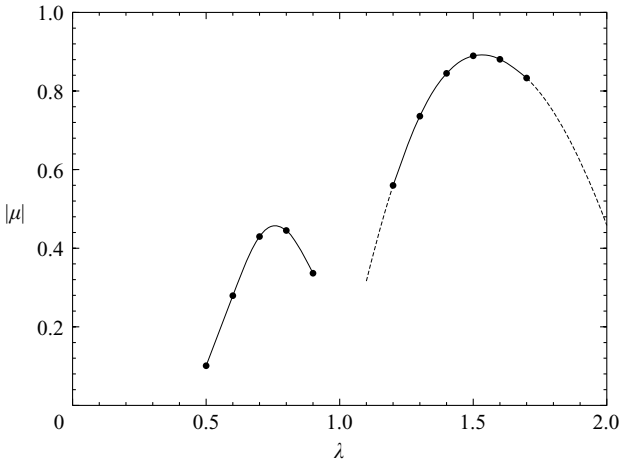

FIGURE 18. Floquet multiplier vs. wavelength when $A^* = 0.75$ and $Re = 230$. Two subharmonic modes are clear; mode SS occupies the bandwidth $0.5 < \lambda < 0.9$ and mode SL occupies $1.0 < \lambda < 2.2$.

A comparison of this figure with figure 14 shows that it is indeed mode SL, and not mode SS, that dominates even at these low values of λ.

For $\lambda > 2.0$, a seemingly quasi-periodic mode exists. This mode seems to have a highly variable period that is dependent on A^*, Re and λ. However, like mode QP emanating from the $2S$ wake mode, it seems to play a secondary role physically, as it never becomes critical before either mode SL or mode SS. It is possible that the role this mode plays increases in importance for other oscillation frequencies.

Increasing the amplitude to $A^* = 0.75$ causes the growth rate of mode SL to decrease enough to allow the resolution of mode SS over the short wavelength range $0.5 < \lambda < 0.9$. Mode SS is clearly present, the relevant change in perturbation-field structure occurring over this wavelength range. The magnitude of the Floquet multiplier is plotted for all wavelengths for this amplitude at $Re = 260$ in figure 18. A comparison with figure 16 shows clearly the emergence of mode SS at this slightly higher amplitude.

The development of each subharmonic mode progresses rapidly over a very small amplitude range, from $A^* = 0.7$ to $A^* = 0.75$; by then the situation has changed dramatically. The major change is that whereas mode SL was completely dominant before, it now ceases ever to reach a critical state and is therefore predicted never to grow. This suggests that, physically, mode SL will have no effect for amplitudes where $A^* > 0.75$. Also, while mode SS still becomes critical, this happens at a significantly higher Re value than for mode SL, at amplitudes only slightly smaller. This effect is made clear through reference to figure 5. A sudden jump in the curve, defining the transition from two-dimensional to three-dimensional flow, is seen to occur at $A^* \simeq 0.72$.

The fact that mode SL never becomes critical at $A^* = 0.75$ is demonstrated by plotting the highest value of μ returned for a given Re, for mode SL at $A^* = 0.75$. Such a plot is shown in figure 19. This shows that initially the growth rate of mode SL increases with increasing Re. However, this trend slows and eventually reverses. Therefore, for $Re > 225$, the growth rate of mode SL decreases with increasing Re. This trend continues so that, at much higher values of Re, mode SL is not resolved at all.

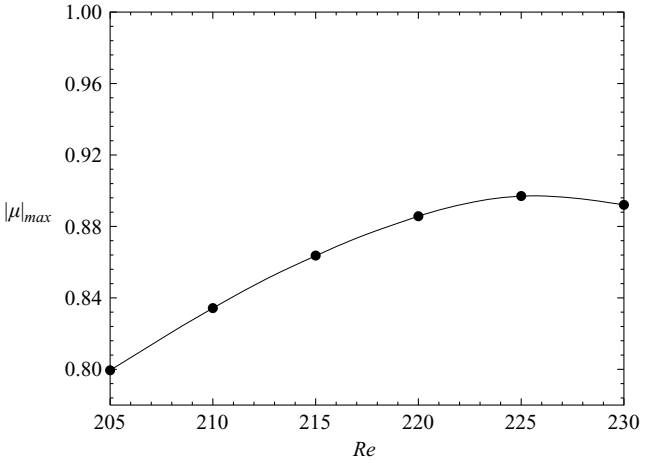

FIGURE 19. Maximum growth rate for mode SL vs. Re when $A^* = 0.75$. It is clear that, for $Re > 225$, the growth rate decreases with increasing Re. It is also clear that the mode never becomes critical.

Further increases in the amplitude of oscillation have the result that mode SL becomes even weaker, leaving mode SS as the only mode that becomes critical. However, increasing A^* has the effect of decreasing the critical Re of mode SS. This is a somewhat non-intuitive result; it seems natural that an increased amplitude of oscillation should have the effect of aligning the wake vortices with the span of the cylinder, strengthening the former and therefore delaying the onset of three-dimensionality. This has been shown to be the case for the $2S$ shedding mode above. However, it does not hold for the $P + S$ shedding mode, and mode SS is seen to become critical at a lower Re as A^* is increased, at least over the range of amplitudes investigated here.

6. Conclusions

Several contributions towards an improved understanding of wakes from oscillating bodies are presented in this paper. Most importantly, the effect of transverse oscillation on the transition to three-dimensionality in the wake of a cylinder has been quantified. It was found that locked oscillation at close to the natural shedding frequency can delay the onset of three-dimensionality until the Reynolds number reaches 280. Furthermore, for $A^* > 0.3$ the transition occurs through a linear mode (mode B) different from for the fixed cylinder (mode A), which possibly strongly affects the transition to fully turbulent flow. This change occurs owing to a damping effect on the initial linear mode due to changes in the scale of the wake vortices.

At higher oscillation amplitudes ($A^* > 0.55$) the two-dimensional base flow changes from a $2S$ to a $P + S$ wake. This alters the three-dimensional transition completely, since modes A and B are bifurcations from the $2S$ state. In fact two new three-dimensional modes arise, modes SL and SS, both of which are subharmonic. For amplitudes where $A^* \lesssim 0.67$, the $P + S$ wake is inherently unstable to mode SL, implying that a two-dimensional $P + S$ wake mode cannot be physically realized over this amplitude range without artificially imposing the restriction to two dimensions.

For amplitudes A^* up to 0.72, mode SL becomes critical first. However, mode SL ceases to become critical for $A^* > 0.72$, leaving mode SS as the first-appearing three-dimensional mode.

Thus four different three-dimensional modes have been shown to lead the transition to three-dimensionality, including two previously unidentified modes, depending on the amplitude of oscillation over the range of amplitudes tested. This may have a profound influence on the routes to turbulence in the different regimes.

REFERENCES

Barkley, D. & Henderson, R. D. 1996 Three-dimensional Floquet stability analysis of the wake of a circular cylinder. *J. Fluid Mech.* **322**, 215–241.

Barkley, D., Tuckerman, L. & Golubitsky, M. 2000 Bifurcation theory for three-dimensional flow in the wake of a circular cylinder. *Phys. Rev.* E **61**, 5247–5252.

Berger, E. 1967 Suppression of vortex shedding and turbulence behind oscillating cylinders. *Phys. Fluids* **10**, S191–193.

Blackburn, H. M. & Henderson, R. 1999 A study of two-dimensional flow past an oscillating cylinder. *J. Fluid Mech.* **385**, 255–286.

Blackburn, H. M. & Lopez, J. M. 2003 On three-dimensional quasiperiodic Floquet instabilities of two-dimensional bluff body wakes. *Phys. Fluids* **15**, L57–L60.

Blackburn, H. M., Marques, F. & Lopez, J. M. 2005 Symmetry breaking of two-dimensional time-periodic wakes. *J. Fluid Mech.* **522**, 395–411.

Griffin, O. M. 1971 The unsteady wake of an oscillating cylinder at low Reynolds number. *J. Appl. Mech.* **38**, 729–737.

Henderson, R. D. 1997 Nonlinear dynamics and pattern formation in turbulent wake transition. *J. Fluid Mech.* **352**, 65–112.

Iooss, G. & Joseph, D. D. 1990 *Elementary Stability and Bifurcation Theory*. Springer.

Julien, S., Ortiz, S. & Chomaz, J.-M. 2004 Secondary instability mechanisms in the wake of a flat plate. *Eur. J Mech* B/*Fluids* **23**, 157–165.

Karniadakis, G. E. & Henderson, R. D. 1998 Spectral element methods for incompressible flows. In *The Handbook of Fluid Mechanics*. CRC Press.

Karniadakis, G. E., Israeli, M. & Orszag, S. A. 1991 High-order splitting methods of the incompressible Navier-Stokes equations. *J. Comput. Phys.* **97**, 414–443.

Karniadakis, G. E. & Sherwin, S. J. 2005 *Spectral/hp Methods for Computational Fluid Dynamics*. Oxford University Press.

Karniadakis, G. E. & Triantafyllou, G. S. 1992 Three-dimensional dynamics and transition to turbulence in the wake of bluff objects. *J. Fluid Mech.* **238**, 1–30.

Koopman, G. H. 1967 The vortex wakes of vibrating cylinders at low Reynolds numbers. *J. Fluid Mech.* **28**, 501–512.

Landman, M. J. & Saffman, P. G. 1987 The three-dimensional instability of strained vortices in a viscous fluid. *Phys. Fluids* **30**, 2339–2342.

Leontini, J. S., Stewart, B. E., Thompson, M. C. & Hourigan, K. 2006 Wake-state and energy transitions of an oscillating cylinder at low Reynolds number. *Phys. Fluids* **18**, 067101.

Leweke, T. & Williamson, C. H. K. 1998 Three-dimensional instabilities in wake transition. *Eur. J. Mech.* B/*Fluids* **17**, 571–586.

Marques, F., Lopez, J. M. & Blackburn, H. M. 2004 Bifurcations in systems with Z_2 spatio-temporal and O(2) spatial symmetry. *Physica* D **189**, 247–276.

Robichaux, J., Balachandar, S. & Vanka, S. P. 1999 Three-dimensional Floquet instability of the wake of square cylinder. *Phys. Fluids* **11**, 560–578.

Ryan, K., Thompson, M. C. & Hourigan, K. 2005 Three-dimensional transition in the wake of bluff elongated cylinders. *J. Fluid Mech.* **538**, 1–29.

Seydel, R. 1994 *Practical Bifurcation and Stability Analysis*. Springer.

Sheard, G., Thompson, M. C. & Hourigan, K. 2003 From spheres to circular cylinders: the stability and flow structures of bluff ring wakes. *J. Fluid Mech.* **492**, 147–180.

Sheard, G., Thompson, M. C., Hourigan, K. & Leweke, T. 2005 The evolution of a subharmonic mode in a vortex street. *J. Fluid Mech.* **534**, 23–38.

Thompson, M. C. 2006 Wake transition of two-dimensional cylinders and axisymmetric bluff bodies. *J. Fluids Struct.* **22**, 793–806.

Thompson, M. C., Hourigan, K. & Sheridan, J. 1996 Three-dimensional instabilities in the wake of a circular cylinder. *Expl Therm. Fluid Sci.* **12**, 190–196.

Thompson, M. C., Leweke, T. & Williamson, C. H. K. 2001 The physical mechanism of transition in bluff body wakes. *J. Fluids Struct.* **15**, 607–616.

Williamson, C. H. K. 1988 The existence of two stages in the transition to three-dimensionality of a cylinder wake. *Phys. Fluids* **31**, 3165–3168.

Williamson, C. H. K. 1996*a* Three-dimensional wake transition. *J. Fluid Mech.* **328**, 345–407.

Williamson, C. H. K. 1996*b* Vortex dynamics in the cylinder wake. *Annu. Rev. Fluid Mech* **28**, 477–539.

Williamson, C. H. K. & Brown, G. L. 1998 A series in $1/\sqrt{(Re)}$ to represent the Strouhal-Reynolds number relationship of the cylinder wake. *J. Fluids Struct.* **12**, 1073–1085.

Williamson, C. H. K. & Govardhan, R. 2004 Vortex-induced vibrations. *Annu. Rev. Fluid Mech.* **36**, 413–455.

Williamson, C. H. K. & Roshko, A. 1988 Vortex formation in the wake of an oscillating cylinder. *J. Fluids Struct.* **2**, 355–381.

Wu, J., Sheridan, J., Welsh, M. C. & Hourigan, K. 1996 Three-dimensional vortex structures in a cylinder wake. *J. Fluid Mech.* **312**, 201–222.